Understanding the Optical Behavior and Spectral Signature of Dredging-Induced Plumes in Coastal Waters

David Doxaran *, Isabella Mayot, Liesbeth De Keukelaere, Robrecht Moelans, Niels Verdoodt, Els Knaeps

Posted Date: 11 February 2026

doi: 10.20944/preprints202602.0865.v1

Keywords: dredging; turbid plumes; spectral signatures; suspended particulate matter; Sentinel2-MSI

 doi:10.20944/preprints202602.0865.v1

Article

Understanding the Optical Behavior and Spectral Signature of Dredging-Induced Plumes in Coastal Waters

David Doxaran [1,*], Isabella Mayot [1], Liesbeth De Keukelaere [2], Robrecht Moelans [2], Niels Verdoodt [3] and Els Knaeps [2]

[1] Laboratoire d'Océanographie de Villefranche (LOV), UMR 7093, CNRS/SU, Villefranche-sur-Mer, FRANCE
[2] Vlaamse Instelling voor Technologisch Onderzoek (VITO), Mol, Belgium
[3] DEME, Scheldedijk 30, 2070 Beveren Kruibeke Zwijndrecht, Belgium
* Correspondence: david.doxaran@imev-mer.fr

Highlights

What are the main findings?

- Particles in suspension in dredge plumes have peculiar (rather spectrally flat) light absorption properties.
- Dredge plumes have a specific spectral signature significantly different from natural turbid waters (e.g., river plumes), i.e., with a higher water reflectance signal at short visible wavelengths (400-550 nm), as detected on water reflectance spectra derived from atmospherically-corrected satellite data.

What are the implications of the main findings?

- Dredge plumes can be identified from ocean colour satellite data, i.e., distinguished from natural turbid waters.
- High spatial resolution (e.g., Sentinel2-MSI) satellite data can be used for the operational monitoring of dredge plumes in coastal waters.

Abstract

Dredging activities regularly occurring in near-shore and coastal waters generate turbid waters within the surface layer with high concentrations of suspended particulate matter collected in bottom sediments. The potential impact of these dredge plumes on natural ecosystems must be monitored using cost-effective methods and observations. Here, we investigate the biogeochemical and optical properties of dredge plumes selected mainly in European and African coastal waters. Laboratory analyses realized on numerous water samples collected in dredge plumes reveal (extremely) high water turbidity and high concentrations of mineral-rich particles in suspension, sometimes mixed to high concentrations of phytoplankton particles. The most peculiar optical property of these particles is a spectral light absorption coefficient significantly flatter than that of suspended particles in natural turbid waters (e.g., river plumes or estuarine maximum turbidity zones). This peculiar optical property is also detected on ocean color satellite data corrected for atmospheric effects, with a water reflectance signal higher than natural turbid waters at short visible wavebands (400-550 nm). Such an atypical spectral signature, that can be detected and mapped from space, makes the operational monitoring of dredge plumes in coastal waters using high spatial resolution (e.g., Sentinel2-MSI) satellite data possible.

Keywords: dredging; turbid plumes; spectral signatures; suspended particulate matter; Sentinel2-MSI

 doi:10.20944/preprints202602.0865.v1

1. Introduction

1.1. Optical Properties and Dredge Plumes

Based on past experience of monitoring dredging sites using satellite and drone data (e.g., [1,2] and references therein), it has become clear that the optical behavior of dredge plumes can differ significantly from that of naturally occurring turbidity (i.e., river plumes, resuspension of bottom sediments by currents). As a result, currently available turbidity algorithms tend to underperform, they can struggle to identify dredge plumes accurately and to quantify turbidity levels effectively.

It is crucial to enhance our understanding of the unique optical properties of these plumes. This will allow to more precisely delineate the spatial extent of dredge plumes and to distinguish them from natural turbidity, a distinction that is critical for environmental assessments in dredging operations. It will also allow the development of dedicated algorithms specifically designed to monitor these dredge plumes in coastal waters.

Currently, environmental monitoring in dredging projects typically relies on a network of sensors (e.g., Conductivity, Temperature and Depth (CTD) and Optical Backscatter Sensor (OBS)), mounted on seabed frames or buoys, to perform more continuous monitoring. These setups are not only labor-intensive to install and maintain, but they also often fail to provide a comprehensive picture of the turbidity impact across a site. Therefore, these assessments have frequently been supported by integrating satellite and drone remote sensing observations combined with in situ measurements. While these Earth Observation (EO) data sources have proven valuable, existing, validated turbidity algorithms often fall short when applied to dredge plumes, underscoring the need for tailored solutions. There is a clear need to better characterize the optical and biogeochemical properties of particles in suspension in dredge plumes. Here, an analysis is presented based on both in situ measurements (and complementary laboratory analyses) combined with the analysis of high spatial resolution ocean color satellite observations.

1.2. Understanding Dredge Plumes

Dredging operations typically involve four main phases [3]: (i) extracting material (ground/sediments) from a specific location, (ii) transporting it to another location, (iii) disposing the material and (iv) returning to the original location. The type of vessels in use depends on many factors but an important one is the type of soil to be dredged: cohesionless soils with small to medium grain size (e.g., silt, sand or fine gravel) are dredged in general with Trailing Suction Hopper Dredgers (TSHD) while cohesive soils (stiff clay) or sediment with large grain size (e.g., boulders) are dredged more often using Cutter Suction Dredgers (CSD) or Backhoe dredgers (BHD). Rock layers are also mainly dredged using CSD. The present study mainly focuses on TSHD operating in areas with silty or sandy soils, as these operations tend to produce the most significant turbidity plumes in surrounding waters.

A TSHD is a self-propelled sea-going vessel equipped with a hold, called hopper, and a dredging installation by which it can fill and/or empty the hopper [3]. This means the TSHD can execute all four steps of a typical dredging operation: trailing (equal to dredging for this dredger type), sailing full (sailing from location 1 to location 2), disposing the sediment and sailing empty (sailing back to location 1). Several options are available for disposing of the material: dumping, pumping ashore or rainbowing (Figure 1).

The trailing part often leads to the turbidity plume with the largest extent, with two main sources of turbidity during this process. While sailing slowly, a draghead is placed on the seabed and a mixture of water and sediment is pumped into the hopper. This process generates turbidity at the seabed, but to a limited extent as the suspended solids remain close to the draghead. While dredging continues, the hopper fills itself with water and sediment. Especially at the start of the operation, the hopper is mainly filled with a lot of water and relatively low amounts of sediment. To be able to transport as much sediment and as little water as possible, the excess water must be discarded. For this purpose, so-called overflows have been installed. These enable the bulk of the sediment to settle

 doi:10.20944/preprints202602.0865.v1

in the hopper while the water and fine particles will flow out [3]. Because the dredging vessel continues to sail and the sediment is released at the water surface, the plume can have a relatively large extent. To control this, the use of the overflow is location-dependent and overflow settings can be adjusted depending on sediment characteristics.

Figure 1. Top view of a dredging vessel (left). View of the rainbowing technique used for sediment disposal (right).

2. Materials and Methods

2.1. In-Situ Data

2.1.1. Field Data Collection

Water samples were collected by DEME at three dredging sites: two in Europe and one in Africa (Table 1). Due to the sensitivity of the data, the exact locations of these sites are not disclosed in this paper. Sampling was carried out using a bucket, either directly inside the hopper or at the water surface near the hopper, several times over a specific time period of about 10 minutes, with the aim of analyzing the optical properties of the dredged materials.

It is important to note that samples taken from inside the hopper are not representative in absolute terms, higher turbidity due to higher concentrations of Suspended Particulate Matter (SPM) will be encountered as a result of the continuous discharge of water. Nevertheless, these samples are considerably easier to collect without interfering with the operational aspects of the dredging activity. Despite this limitation, they are valuable for deriving the specific optical absorption and backscattering properties of the dredged materials before their release in natural waters, where mixing with ambient material and rapid sinking of the coarse SPM will occur.

Immediately after collection, four clean 1-liter dark plastic sampling bottles were filled. The bottles were placed in a cool box with cold packs and transported within 48 hours to the laboratory in France for further analyses.

Table 1. Site locations, sampling dates and number of water samples collected in each dredging site.

Site	Date of field data collection (ID)	Comments
Dredging Site 1 Europe (D1EU)	19/11/2024 (D1EUa)	Dredging with TSHD. 3 water samples collected from tender boat near the hopper
	17/12/2024 (D1EUb)	Dredging with TSHD. 5 water samples collected near the hopper
	11/02/2025 (D1EUc)	Dredging with TSHD. 8 water samples collected, including 4 in the hopper, 4 near the hopper
	17/03/2025 (D1EUd)	Dredging with TSHD. 5 water samples collected, 3 in the dredge plume, 2 outside the dredge plume. All taken near the hopper

 doi:10.20944/preprints202602.0865.v1

Dredging Site 2 Europe (D2EU)	24/04/2025 (D2EUa)	Dredging with CSD. 6 water samples collected, 3 on starboard side and 3 on the port side, near the vessel
	04/06/2025 (D2EUb)	Dredging with CSD. 8 water samples collected, 4 starboard side, 4 port side, near the vessel. A barge was being loaded alongside CSD on port side, and so samples were taken between CSD and barge. The barge was utilizing overflow.
	17/06/2025 (D2EUc)	Dredging with CSD. 8 water samples collected, 4 starboard side, 4 port side. CSD was cutting starboard. Samples were taken during dredging of the CSD while loading a TSHD with floating line – bow coupling connection.
Dredging Site 1 Africa (D1A)	30/11/2024 (D1Aa)	Dredging with TSHD. 7 water samples collected, including 1 (reference) before dredging, and 2 in the hopper
	13/02/2025 (D1Ab)	Dredging with TSHD. 8 water samples collected, including 4 inside the hopper

2.1.2. Analyses of Water Samples in Laboratory

On the day the water samples were delivered, they were analyzed in LOV facilities to determine the optical and biogeochemical properties of suspended particles, in order to determine how these properties influence the aquatic reflectance signal and how they differ from that of SPM in natural turbid waters.

Prior to any filtration or analysis, the water samples were gently shaken in order to obtain a homogeneous concentration of suspended particles in each bottle (Figure A1). The first optical property measured was the water turbidity (TU, in Formazin Nephelometric Unit (FNU)). A portable HACH 2100Q turbidimeter was used. This bench instrument records turbidity between 0 and 1000 FNU. A 10-ml vial containing the water sample is illuminated by a light-emitting diode with emission at 860 ± 60 nm. The instrument measures turbidity via the ratio of light scattered at an angle of 90° ± 2.5° to forward- transmitted light as compared to the same ratio for a standard suspension of Formazin. We followed the protocol described in [4]: turbidity was recorded in triplicates that were averaged and used to estimate the measurement uncertainty as the associated standard deviation between triplicates. Turbidities of the STABLCAL Stabilized Formazin Turbidity 10 or 20, 100 and 800 FNU standards and that of pure water were recorded after each day of laboratory analyses to check the instrument stability. In some cases, especially when water samples were collected within the hopper, the initial turbidity could exceed 1000 FNU (Figure A2). Although the absolute values of samples collected within the hopper do not reflect the actual turbidity levels of the dredge plumes, as the hopper continuously discharges water, these measurements were nonetheless acquired. For such extremely high turbidity values (>1000 FNU), water samples were diluted with pure (Milli-Q) water to bring them within the 0-1000 FNU measurement range. This occurred:

- D1A: in two samples (out of seven) collected in November 2024 in the dredging site 1 in Africa (dilutions of 1 in 10 and 1 in 50);
- D1A: on the same site in February 2025 (all samples collected had to be diluted 10 times);
- D1EU: in the dredging site 1 in Europe in November 2024 (one sample diluted 10 times), then in February 2025 (four samples out of 8 had to be diluted two times);
- D1EU: on the same site in December 2024 (water samples had to be pre-filtered at 200 µm to remove coarse (sand) materials then diluted 2 to 10 times.

 doi:10.20944/preprints202602.0865.v1

This highlights the difficulty in analyzing such potentially extremely turbid water samples containing mixtures of coarse and fine bottom sediments. Note that these difficulties were not encountered with the water samples collected on site D2EU, associated with much lower turbidity values.

Following recommendations made by [5], the measured turbidity values were used to optimize the volume of water sample (V, in m^3) to be filtered for determination of the SPM concentration (SPM, in $g.m^{-3}$). As in [6], pre-ashed and pre-weighed Whatman GF/F filters (25 mm, 0.7 µm pore size) were used in triplicates to filter the water samples. Filters were then dried 24 hours at 60°C and weighed in a dry environment to determine the dry mass of SPM (m_1, in g), so that the SPM concentration in $g.m^{-3}$ was obtained as:

$$SPM = (m_1 - m_0) / V, \quad (1)$$

With m_0, in g, the initial mass of the dry GF/F filter.

The exact same triplicates of filters were finally combusted for 4 h at 450°C and weighed again to determine the mass of inorganic particles (m_2, in g), thus by difference, the respective fractions of SPM (here called Particulate Organic and Inorganic Fractions (POF and PIF, in %) [7,8]:

$$PIF = (m_2 - m_0) / (m_1 - m_0) \times 100 \text{ and } POF = 100 - PIF. \quad (2)$$

The same volume of water as for SPM was filtered for subsequent high-performance liquid chromatography (HPLC) analyses by the SAPIGH French service (https://lov.imev-mer.fr/web/facilities/sapigh/) to determine the concentrations of 26 phytoplankton pigments [9], including the concentration of total chlorophyll-a (Chla, $mg.m^{-3}$), a proxy of the phytoplankton biomass (analyses done on D1EU, D1A and D2EU samples).

Lastly, the light absorption coefficients of total, non-algal and algal particles (respectively a_p, a_{nap} and a_{phy} in m^{-1}) were measured with a spectrophotometer (Perkin-Elmer Lambda 850 UV/VIS) equipped with an integrating (Spectralon) sphere (150 mm diameter), following the last International Ocean-Colour coordinating Group (IOCCG) protocol [10]. The filters were first placed in the center of the sphere to measure a_p from 400 to 800 nm, with a spectral resolution of 1 nm. Filters were then put for one hour in a filtration funnel filled with methanol to dissolve the phytoplankton pigments and the absorption coefficient (a_{nap}) of the remaining particles (called non-algal particles) was measured in the center of the sphere. The absorption coefficient of the phytoplankton particles (a_{phy}) was finally obtained as the difference:

$$a_{phy} = a_p - a_{nap}. \quad (3)$$

Depending on the dredge site, the contribution of algal particles was usually observed to be negligible but sometimes proved to be surprisingly very significant in such turbid waters (Figure A3). The a_{nap} coefficient was modeled as [11]:

$$a_{nap}(\lambda) = a_{nap}(443) \times e^{-Snap(\lambda - 443)} + B, \quad (4)$$

With λ the wavelength in nm, B the non-negligible light absorption coefficient at 800 nm and *Snap* the spectral slope (in nm^{-1}) which contains information concerning the composition thus origin of the non-algal particles [12].

2.2. Satellite Data Processing

2.2.1. Selection of Sentinel-2 Images

DEME compiled a list of globally distributed dredging sites since 2016 where data from TSHD operations and/or in situ turbidity measurements are available. For these selected locations, corresponding Sentinel-2 (S2) Multi Spectral Imager (MSI) images were downloaded and processed using the Terrascope water processor. MSI data from both S2A and S2B satellite platforms were considered. To ensure high quality data for further analysis, S2-MSI images with cloud cover

 doi:10.20944/preprints202602.0865.v1

obscuring the dredging area were manually discarded. While the metadata includes a cloud cover percentage for the entire S2 tile, this often leads to misinterpretations – for example, a high cloud cover percentage may be reported even when the specific area of interest remains unobstructed. Additionally, the IDEPIX-based pixel classification, integrated in Terrascope, is not always accurate, occasionally misclassifying water pixels. To address these limitations a manual screening approach was adopted using the Copernicus Data Space Ecosystem browser, enabling more reliable visual assessment and image selection.

To investigate the spectral properties of dredge plumes, the two European sites and the African site were used next to additional sites with well-defined and distinguishable plumes. As a result, three additional dredging locations were selected:

- Dredging site 2 Africa (D2A)

This site was selected due to the extensive and diverse dredging activities conducted over an extended period (01/01/2021 - 31/12/2025) [13,14], including TSHD and CSD operations, pumping ashore, and rainbowing [13]. Moreover, a substantial number of high-quality satellite images are available thanks to consistently favorable weather conditions and low cloud cover.

- Dredging site 1 Russia (D1R)

D1R was chosen for its well-defined and visually distinct dredge-turbidity plumes. These plumes occur in relatively clear waters with low natural background turbidity, making them ideal for analysis. At various times, two to three TSHDs operated simultaneously at this location, making it an interesting dataset for studying plume formation and dynamics under different dredging conditions. S2-MSI data of the corresponding tile was processed from 01/07/2019 - 01/06/2020.

- Dredging site 3 Europe (D3EU)

The D3EU site, notably known for its dredged material dumping sites [15], was selected as a study site due to its location in colored dissolved organic matter (CDOM)-rich waters, which significantly influences the spectral properties of water. Understanding whether and how CDOM affects the appearance characteristics of dredge-induced plumes is essential for accurate remote sensing analysis. Additionally, the presence of natural sediment plumes from nearby river outflows provides an opportunity to compare and differentiate between dredge-generated and naturally occurring turbidity features. S2-MSI data from the corresponding tile were processed for the period 03/11/22 - 24/10/2023.

2.2.2. Atmospheric Correction of S2-MSI Images

The operational ICOR atmospheric correction approach was selected for processing the S2-MSI images and is described in the next section. However, to quantify the impact of the atmospheric corrections applied to S2-MSI satellite data on the retrieved aquatic reflectance (AR [https://ceos.org/ard/files/PFS/AR/v2.0/CEOS-ARD_Product_Family_Specification_Aquatic_Reflectance-v2.0.pdf], i.e., the spectral signature notably of the dredge plumes), a selection of S2-MSI satellite images from different test sites were processed using the iCOR [16], ACOLITE-DSF [17] and Sen2Cor processors [18] for intercomparison (e.g., Figure A4). These three atmospheric correction algorithms were proved to be amongst the most accurate over (highly) turbid waters [19] and are operational for S2-MSI data. S2A&B-MSI L1C (for ACOLITE processing) and L2A (Sen2Cor product) satellite data were downloaded from the Copernicus web site (https://browser.dataspace.copernicus.eu). iCOR, ACOLITE and Sen2Cor-derived AR spectra on same images were extracted on a number of locations along and outside identified dredge plumes and compared as spectral signatures and scatterplots over the visible and near-infrared spectral ranges (400 – 900 nm) (Figure A5).

 doi:10.20944/preprints202602.0865.v1

2.2.3. ICOR Atmospheric Correction Using Terrascope

The atmospheric correction of S2 imagery was performed using the operational Terrascope implementation of iCOR [16]. The full correction workflow, as realized within Terrascope, is depicted in Figure 2. This systematic approach ensures the generation of accurate AR products, which are crucial for downstream analyses of aquatic environments.

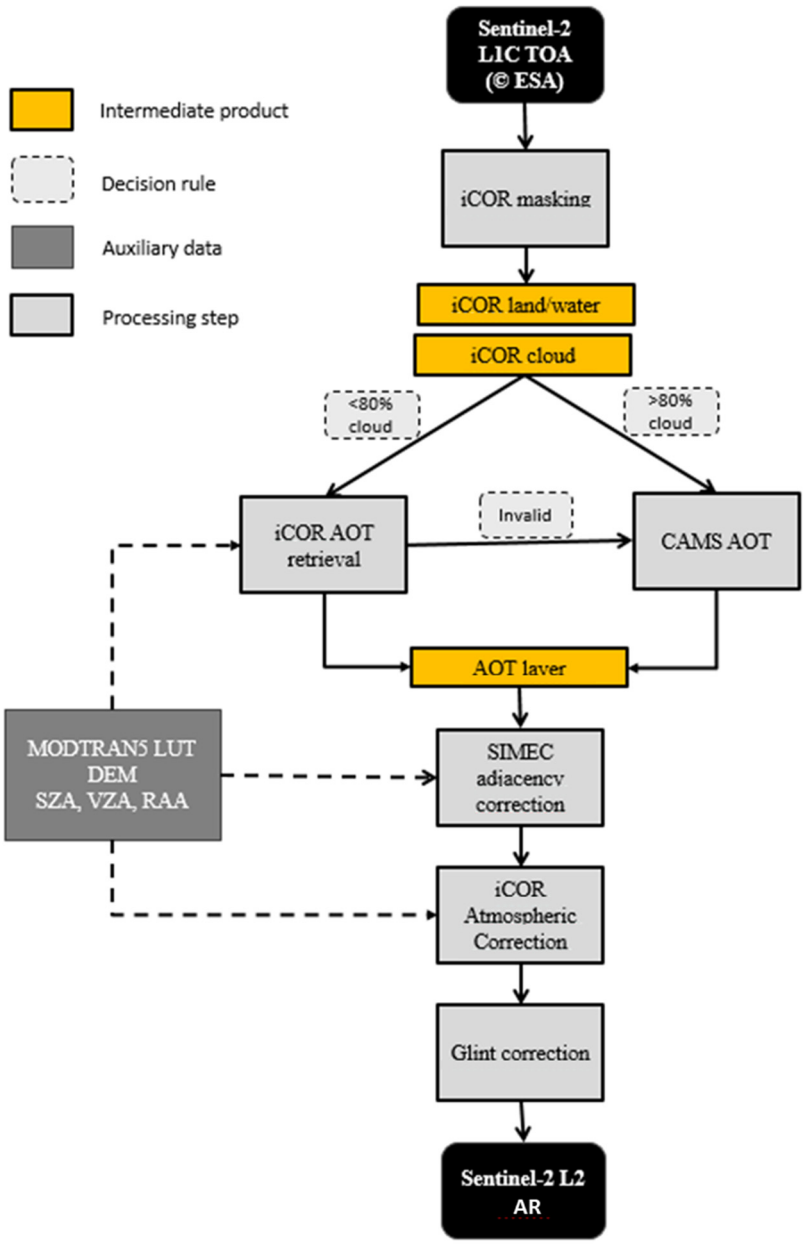

Figure 2. Workflow of iCOR implemented in the Terrascope processing chain. The iCOR aerosol optical thickness (AOT) retrieval is invalid when the absence of clear land pixels hampers an accurate image-based AOT retrieval.

The process initiates with S2 Level-1C Top-of-Atmosphere (TOA) reflectance products. An initial masking step is applied using iCOR, which generates intermediate land/water and cloud mask layers. These layers are critical inputs for both Aerosol Optical Thickness (AOT) retrieval and the final atmospheric correction. In addition, the discrimination between land and water surfaces allows an additional sky glint correction over water bodies to mitigate the influence of reflected skylight.

 doi:10.20944/preprints202602.0865.v1

The land-water mask is established through a thresholding approach applied to the TOA reflectance signal in the near-infrared (NIR) band at 10 m resolution. Pixels exhibiting TOA reflectance values below 0.05 in Band 8 (842 nm) are classified as water. The resulting land-water mask, initially produced at 10 m resolution, is subsequently resampled to 20 m and 60 m resolutions via nearest-neighbor resampling using the GDAL library, ensuring spatial consistency across bands.

For cloud detection, an internal algorithm is employed during the atmospheric correction step, in contrast to standard cloud masks such as those provided by Sen2Cor or IdePix. This tailored algorithm is designed to prioritize the over detection of clouds, thereby enhancing the accuracy of AOT estimation. The approach, grounded in the method proposed by [20], is compatible with any sensor equipped with visible and near-infrared (VNIR) spectral bands.

Following pixel identification and masking, the retrieval of AOT values at 550 nm is performed either directly from the S2-MSI imagery via iCOR or, when necessary, supplemented with external datasets. By default, AOT retrieval from the image data itself is favored, provided that conditions are adequate for accurate derivation [16]. However, in cases where cloud cover exceeds 80% or the derived AOT is unreliable—such as when there is insufficient land coverage or spectral diversity—external AOT data sources are utilized. The preferred external dataset is the Copernicus Atmosphere Monitoring Service (CAMS) Near Real Time (NRT) product, provided by the European Centre for Medium-Range Weather Forecasts (ECMWF) [21,22]. In exceptional cases, where the temporal difference between the S2 acquisition and the availability of CAMS NRT data exceeds 24 hours (for instance, due to server connectivity issues), CAMS climatological monthly averages are employed as fallback [22].

An essential component of the atmospheric correction workflow is the application of the SIMilarity Environment Correction (SIMEC) algorithm [23]. This correction compensates for adjacency effects, which occur when the radiance signal from dark targets, such as inland water bodies, is contaminated by the reflectance from adjacent bright surfaces like land. SIMEC effectively mitigates this phenomenon, ensuring that the reflectance of dark targets remains true to their actual surface properties.

The final atmospheric correction integrates multiple inputs: the land/water and cloud masks, AOT layers, MODTRAN5 look-up tables (LUTs), a digital elevation model (DEM), and solar and viewing geometries averaged from the angular information contained in the S2-MSI metadata. These elements collectively enable the iCOR atmospheric correction process, yielding high-quality AR products from the S2-MSI imagery, suitable for aquatic ecosystem analysis and monitoring.

3. Results

3.1. Satellite Intercomparison of Atmospheric Corrections

Figure A4 shows a typical comparison made between a S2-MSI image processed using ACOLITE, iCOR and Sen2COR. Over most of the image, the water is clear, but several types of turbidity structures appear: natural ones and, on the top left, an area of intensive dredging activities. In terms of spatial variations of aquatic reflectance but also magnitude of the AR signal (here at 560 nm), the agreement is obvious between iCOR and ACOLITE products. By contrast, the AR signal retrieved using the Sen2Cor algorithm is significantly higher over the clearest to moderately turbid waters. These first qualitative comparisons tend to highlight the limits of the Sen2Cor algorithm initially not designed for the retrieval of water quality parameters but for land applications.

The good agreement between iCOR and ACOLITE water products is confirmed when extracting AR spectra inside and outside dredge plumes in various test sites across the globe (Mexico, Russia, Nigeria, Abu Dhabi and the UK). (Figure A5). AR spectra are typical of moderately to highly turbid waters [28]. Scatterplots confirm the very good agreement between iCOR and ACOLITE products especially at 560 nm (where the water-leaving signal is maximum), with a best-fitted linear relationship having a slope of 1.05, a negligible intercept and a determination coefficient close to 1 (Figure A5). This agreement when considering several S2-MSI images and wavebands in the visible

 doi:10.20944/preprints202602.0865.v1

and NIR spectral ranges, with differences lower than 8% on average. These results clearly tend to validate the iCOR atmospheric correction processing, which allows retrieving AR spectra very close to those obtained by applying the ACOLITE-DSF approach, which has been proven to perform well in turbid waters (e.g., [19]).

The results obtained are clearly not as satisfactory when comparing Sen2cor-derived AR values to ACOLITE products (here used as a reference) (Figure A6). The best-fitted linear relationship has a much lower determination coefficient ($R^2 = 0,53$), and the overall difference is close to 40% on average over the VNIR spectral regions, with Sen2Cor-derived AR values overestimating those retrieved using ACOLITE.

The conclusion at this stage is that both iCOR and ACOLITE processors can be used to retrieve the spectral signature of turbid waters inside and outside dredge plumes, while Sen2Cor products should be avoided.

The next step is to analyze and compare the spectral signatures of (highly) turbid waters encountered in natural environments such as estuaries and in dredging plumes. Figures A7 and A8 illustrate such comparisons considering ACOLITE-derived AR spectra respectively extracted from Landsat8 Operational Land Imager (OLI) and S2-MSI satellite data in the highly turbid Gironde Estuary (France) and in the Russian dredge site considered in the present study. The AR values in natural environments is significantly higher at short visible wavelengths (< 560 nm) and greatly higher in red to NIR wavelengths (> 600 nm) for a similar AR signal at 560 nm. The AR signal at short visible wavelengths clearly tends to saturate (as already described by [24]) but apparently not in dredge plumes. At equivalent SPM concentration or water turbidity, this could result from different SPM size distributions, with finer SPM in natural waters resulting in enhanced light absorption at short visible wavelengths (thus lower AR values) and lower light absorption by SPM at longer wavelengths (thus higher AR values). Such an assumption should, however, be confirmed by field measurements or laboratory analyses.

Similar observations can be made at the top of the atmosphere when comparing S2-MSI data recorded over naturally-turbid waters and dredge plumes (Figure A9). TOA reflectance values (Rhot) computed using ACOLITE show rather smooth spectra over dredge plumes with Rhot values decreasing with increasing wavelengths (typical of the atmospheric signal) together with a signal significantly increasing with increasing water turbidity over the visible spectral region (400-700 nm). In the naturally-turbid Gironde estuarine waters, the Rhot signal is quite different with very limited variations at short visible wavelengths and by opposition maximum variations observed in the red and NIR spectral regions, which is typical of highly scattering waters, probably resulting from the high concentrations of fine mineral-rich particles.

3.1. In-Situ Data Analysis

Table A1 summarizes the biogeochemical and optical properties of particles in suspension in the dredge plumes, based on water samples collected in the field and subsequent laboratory analyses. Once on two sites (D1EU and D1A), the same properties were measured on “reference” water samples, i.e., a water sample collected either before release of the dredging plume (D1A) or outside the dredge plume (D1EU), in order to highlight the differences between natural particles in suspension and particles released by dredging activities. The biogeochemical and optical properties are reported for each site (D1EU, D2EU and D1A) as minimum, maximum, and mean values, keeping in mind these sites were respectively sampled 4 and 2 times over the years 2024 and 2025.

In the first European site (D1EU), the SPM concentration within surface waters was observed to vary from 223 to 1381 $g.m^{-3}$, with a mean value around 750 $g.m^{-3}$. Outside the dredge plumes, the “natural” SPM concentration was close to 30 $g.m^{-3}$, i.e., 10 times lower than the minimum concentration measured in the plumes. By opposition, in D2EU, lower SPM concentrations were obtained, ranging from 5 to 28 $g.m^{-3}$ with a mean value of 11 $g.m^{-3}$. Much higher SPM concentrations were measured in water samples collected in the hoppers at both the African dredge site (D1A), with an extremely high concentration close to 30000 $g.m^{-3}$, and concentrations of 1 to several thousands of

 doi:10.20944/preprints202602.0865.v1

g.m^{-3} often measured (measurements obtained after dilutions), and in D1EU in Europe. When discharged from the hopper into coastal waters, dilution occurs so that SPM concentrations in dredge plumes rapidly reach values of 300 to 100 g.m^{-3}, i.e., SPM concentrations found within surface waters of natural environments such as river plumes or macro-tidal estuaries (e.g., [25,26]).

As expected, the organic and inorganic fractions of SPM revealed the predominance of mineral-rich particles in dredging plumes, with particulate inorganic fractions (PIF) typically ranging from 85 to 95% (Table A1), indicating still a significant amount of organic matter of unknown origin (terrestrial or locally-produced by phytoplankton).

The water turbidity values measured on both sites showed a clear correlation with measured SPM concentrations, with as a first approximation a best-fitted linear relationship having a slope close to 1, as usually reported in naturally turbid waters [27]. To be more precise, analyzing the variations of the turbidity to SPM concentration ratio is interesting to document how efficient are suspended particles in dredge plumes in terms of light scattering, as compared to particles in suspension in natural environments. On both sites, this ratio has proven to be significantly higher in dredge plumes, with values from 0,7 to 1,1 FNU.m^3.g^{-1}, than in surrounding waters (0,3 FNU.m^3.g^{-1}). This can be explained by the predominance of mineral-rich SPM in dredge plumes associated with a high refractive index compared to mixed mineral and phytoplankton particles found in natural waters.

This assumption is actually confirmed by the measured contributions of non-algal particles to the total particulate light absorption coefficient in D1EU and D1A dredge plumes (Figure A3): these contributions appeared to vary from 90 to 100% at 443 nm (a wavelength corresponding to a peak of light absorption by phytoplankton pigments) [12]. In surrounding waters, this contribution was observed to be 10 to 30% lower (Table A1). The light absorption coefficients measured in D2EU actually appear to be very similar to absorption spectra documented in natural coastal waters, with an unexpected very significant contribution of phytoplankton pigments [12]. Moreover, the SPM mass-specific absorption coefficient of non-algal particles at 443 nm ($a_{nap}(443)$, in m^2.g^{-1}) did not differ from typical values reported for a wide range of European coastal waters [12]. By contrast, the spectral slope associated with the measured a_{nap} spectra has proven to be peculiar, i.e., quite at the extreme limit of values reported by [12] in natural European coastal waters. The S_{nap} values measured in the dredge plumes actually varied from 0,007 to 0,010 nm^{-1}, which is at the extreme lower limit of values reported by [12]. As SPM sampled in dredge plumes were found to be mineral-rich, this most probably indicates the presence of coarse SPM not efficient in terms of light absorption at short visible wavelengths, but significantly absorbing light in the NIR. This peculiar light absorption by non-algal particles in dredge plumes most probably explains the specific spectral signatures (AR spectra) observed in dredge plumes compared to that of naturally turbid waters (Figures A7 and A9) and can represent a way to distinguish and identify dredge plumes from ocean color satellite data (Figure A9). A significant part of suspended particulate matter in dredge plumes have been observed to be phytoplankton particles, mainly diatoms, based on HPLC analyses.

3.2. Analysis of Aquatic Reflectance Spectra

To evaluate differences in spectral characteristics between natural waters and plumes resulting from dredging activities, S2 images were selected based on the presence of clearly identifiable dredge-induced plumes. These images represent geographically diverse sites and capture distinct dredging operations.

The first image, acquired on 10 February 2021 over D2A, depicts intensive dredging activity involving approximately four hopper dredgers with clearly visible plumes. Additionally, rainbowing operations are visible near the coastline. The second image, acquired on 14 February 2023, covers the D3EU, where active dredging plumes are also apparent. The third image, from 21 October 2019, captures the coastal area of D1R, where sediment disturbance is linked to visible dumping operations. Figure 3 shows the dredging activities observed in the corresponding S2 images.

For the dredging sites in Europe and Africa, where field sampling has been performed, four S2 images have been selected. For D1A dredging plumes were clearly visible in the images captured on

 doi:10.20944/preprints202602.0865.v1

15/11/2024 and 30/11/2024. For the two European sites, images of the dredging activity were captured on 21/03/2025 and 16/05/2025 but dredging plumes were small and less visible (Figure 4).

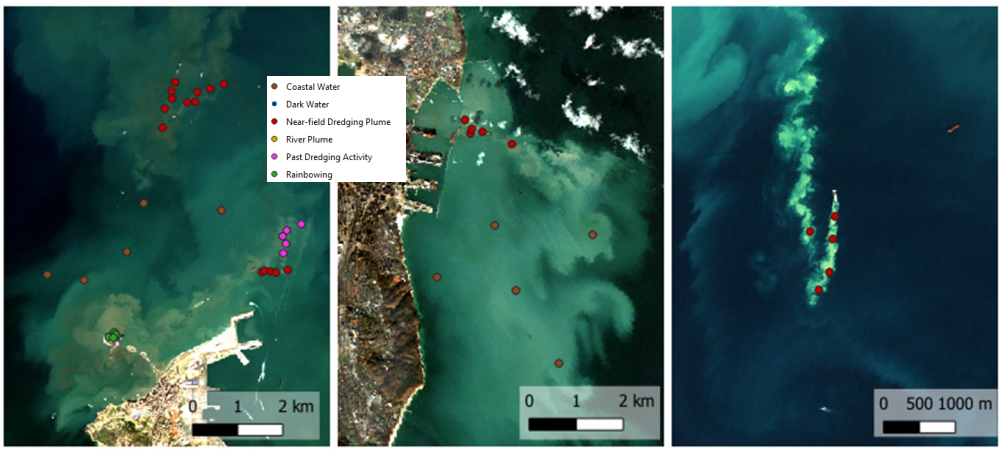

Figure 3. Dredging activities observed in S2 imagery over D2A (10/02/2021, left), D3EU (14/02/2023, middle), and D1R (21/10/2019, right).

Figure 4. Dredging activities observed in S2 imagery over Dredging Site 1 Africa (D1A, 15/11/2024 and 30/11/2024, left). Dredging Site 1 Europe (D1EU, 21/03/2025, middle) and Dredging site 2 Europe (D2EU, 16/05/2025, right).

For all sites, spectra were extracted in the dredge plumes very close to the dredging vessel (near-field dredging plume), further from the dredging vessel (far-field dredging plume), in nearby coastal waters, dark waters and river plumes. In some cases, special categories were included such as rainbowing and past dredging activities when present in the scene. Figure 5 shows an overview of the AR spectra extracted for the different sites. Each spectrum represents an average of 4-5 spectra as indicated in the figure (n=5 or n=4), and the shaded area shows the range between the minimum and maximum values. As a reference, a selection of AR spectra of turbid and very turbid waters from the SeaSWIR database [28] have been added in light grey. These present AR spectra collected with an ASD spectrometer from the Scheldt, La Plata and Gironde estuaries with SPM concentrations ranging between 49 and 917 $g.m^{-3}$.

The following observations can be made:

- The Dark water category in blue exhibits low reflectance across the spectrum, with a slight increase in the blue-green region. This spectral shape is characteristic of clear water bodies with minimal optically active constituents such as suspended sediments or phytoplankton, suggesting low turbidity and low biological activity;
- Spectra collected in the River Plume category (yellowish) show elevated reflectance compared to Dark water, particularly in the green and red spectral regions. However, in the blue region,

 doi:10.20944/preprints202602.0865.v1

reflectance values drop significantly, which may indicate strong absorption due to non-algal particles, phytoplankton or dissolved organic matter. In D2A, this is further supported by a small observed dip around 665 nm, a known absorption feature associated with chlorophyll-a, suggesting biological influence and a potential presence of algal matter;

- Rainbowing (D2A only) results in a relatively flat spectral response across the visible spectrum, with elevated reflectance extending into the NIR region. This suggests a particle-rich composition, rather than a water-dominated one, as water typically exhibits stronger absorption, particularly in the NIR spectral region;
- Near-field dredging plumes (dark red) exhibit the overall highest reflectance values, indicating a high concentration of suspended sediments and strong light scattering. They have a pronounced peak near 560 nm and sustained high values into the NIR. However, compared to very turbid riverine waters from the SeaSWIR database (e.g., [26];[28]), these spectra specifically show a higher reflectance in the blue and green and lower values in the NIR. This could potentially be related to lower CDOM, NAP and Chla absorption compared to the riverine waters. For D2A, the near field dredging plume consists of plumes from three different hoppers (see Figures 6 and 7: hoppers 1, 2 and 3). The plume from past dredging activity is probably linked to dredging activities from hopper 1 with hopper 1 having the highest reflectance values. This explains the higher reflectance from the past dredging activity. For D2EU, the near-field dredge plume spectrum is overall lower with slight difference with the spectrum from surrounding coastal waters. This is probably due to the small size of the dredge plume, different dredging technique (CSD) and difficulty to extract the spectra from the dredge plume accurately. The spectra probably represent mixed cases;
- In the case of far-field dredging plumes (bright red), a noticeable decline in reflectance is observed, suggesting sediment settling, plume dispersion and mixing with other water types over time. This temporal change may reflect a reduction in particle concentration or shifts in particle composition as the plume ages.

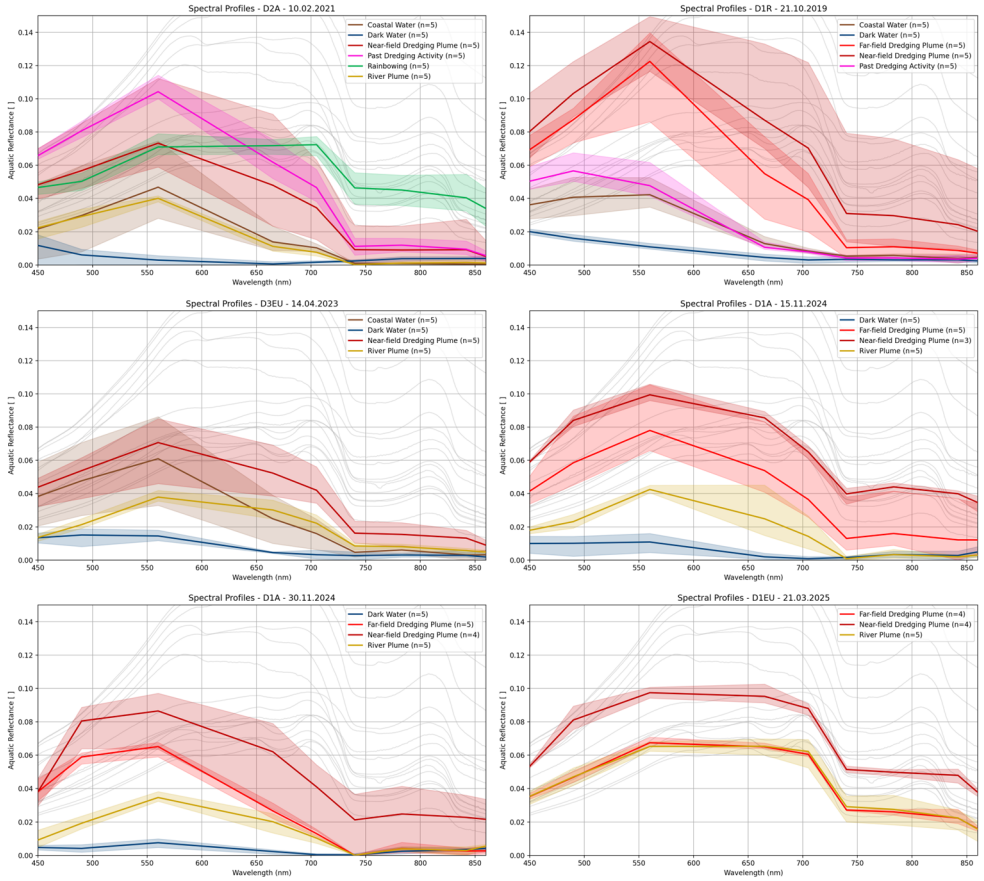

 doi:10.20944/preprints202602.0865.v1

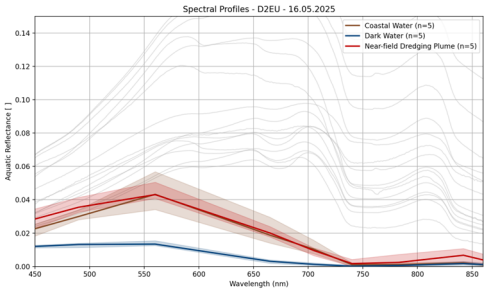

Figure 5. Typical aquatic reflectance (AR) spectra extracted from S2-MSI images in various locations of the different dredging sites considered.

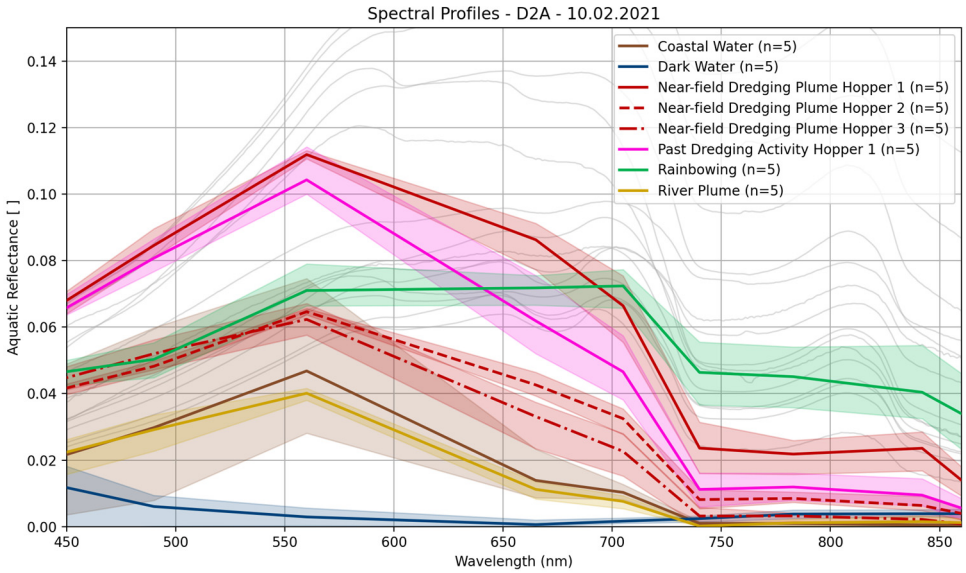

Figure 6. Typical aquatic reflectance (AR) spectra extracted from S2-MSI images of Abu Qir considering different hoppers.

 doi:10.20944/preprints202602.0865.v1

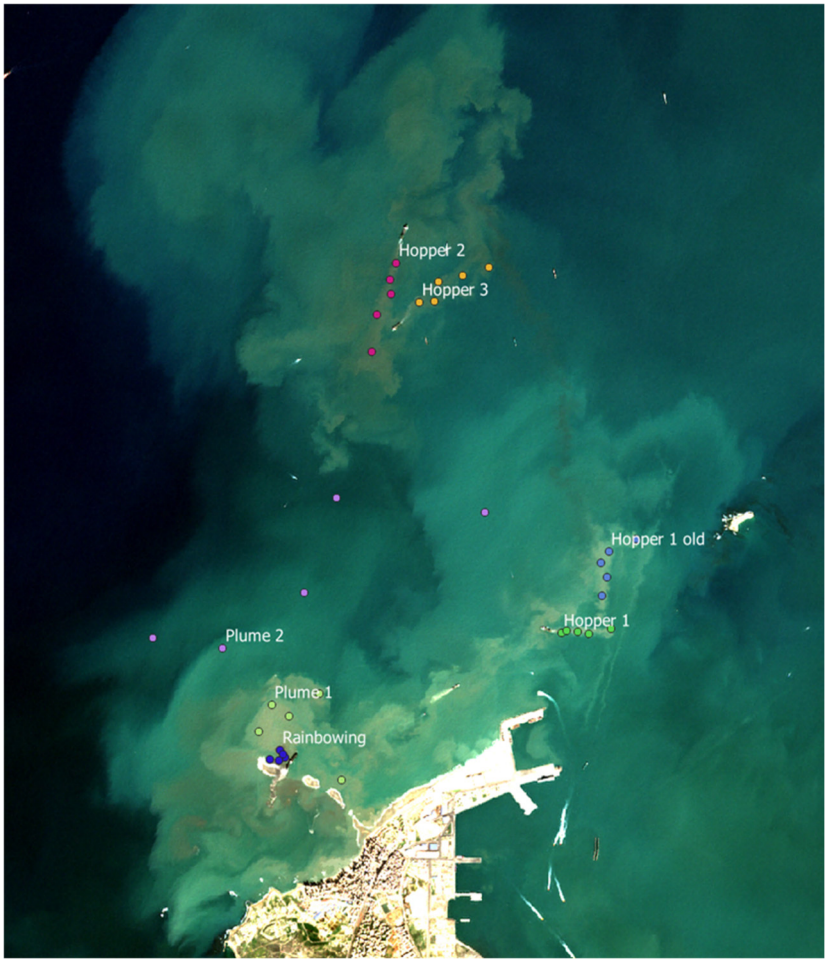

Figure 7. S2 image showing the different hoppers active in the area and the associated dredge plumes.

4. Discussion and Conclusions

The present study combined biogeochemical and optical laboratory analyses of water samples collected in the field in several dredging sites, in the hopper, then inside and outside the dredging plumes, with S2-MSI atmospherically-corrected satellite observations of the spectral signatures of dredging plumes, surrounding clear waters and naturally turbid waters over several representative dredging sites. The objective was to highlight the differences between dredge plumes and natural waters, in order to help develop a robust and operational remote sensing algorithm to identify, map and monitor the dynamics of dredge plumes in turbid coastal waters.

As expected, waters in dredge plumes are associated with high turbidity and high concentrations of mineral-rich SPM, but also, surprisingly, sometimes exhibit the presence of phytoplankton particles (Table A1). The associated SPM-specific turbidity (i.e., light side-scattering (turbidity, TU) per unit of SPM concentration) revealed values typical of mineral-dominated particles, with a stable TU/SPM ratio close to 1 (Table A1, [28]). The corresponding light absorption coefficient per unit of SPM concentration showed values typical of turbid coastal waters [12] but a peculiar spectral slope with quite stable values (of about 0,009 nm^{-1}) which correspond to minimal values reported in a wide range of European coastal waters [12]. This certainly reveals the presence of mineral-rich particles coarser than natural suspended particles (clays and silts).

Intercomparisons between three different approaches used to correct S2-MSI satellite data for atmospheric effects showed the good consistency of results obtained using the iCOR and ACOLITE processors, i.e., two algorithms specially designed for turbid waters. These results proved the reliability of the spectral signatures of dredge plumes and surrounding turbid and clear waters extracted from satellite data processed using iCOR. It offered the opportunity to extract the spectral shape (aquatic reflectance spectra) from a wide range of dredge plumes, naturally clear and turbid

 doi:10.20944/preprints202602.0865.v1

waters in different sites (Figures 4 to 9). The spectral signatures of dredge plumes can easily be distinguished from surrounding clear waters simply due to the strong difference in terms of the magnitude of the signal, with typically a factor 4 to 10 over the visible to NIR spectral domains (Figures 5 and 6). The aquatic reflectance of clear waters shows respectively low and negligible values in the visible and NIR, while dredge plumes waters exhibit a high signal in both spectral regions. Interestingly, the aquatic reflectance of dredge plumes is also clearly higher than that of naturally-turbid waters observed on the selected test sites (Figures 5 and 6). Now considering extremely turbid waters in natural environments such as macro-tidal estuaries and river mouths, the spectral signatures are, at first glance, quite similar, at least in the red to NIR spectral regions, both in terms of spectral variations and magnitude (e.g., [26], Figures A7 and A8). However, a significant difference can be highlighted at short visible wavelengths (400-550 nm), where the magnitude of the aquatic reflectance signal mainly depends on light absorption by non-algal particles. Comparing the spectral shapes of dredge plume waters (Figure 4, 6 and 8) to that of highly turbid estuarine waters ([24] and Fig. 4 in [26]), the typical signature of dredge plumes clearly shows a significantly higher magnitude between 400 and 500 nm. The most probable explanation of this difference is the peculiar spectral slope of the particulate light absorption coefficient in dredge plumes. This spectral slope is systematically lower than in natural coastal waters (Table A1 and [12]), which results in a minimum light absorption by particles at short visible wavelengths, thus a significantly higher aquatic reflectance signal. These different light absorption properties most probably result from differences in terms of particle size distributions, with bigger (coarser) particles in dredge plumes than in natural waters; this assumption still requires to be confirmed based on field measurements.

The results reported in this study, based on laboratory analyses of field water samples and multi-spectral satellite observations of dredge plumes and surrounding waters, are promising as they showed dredge plumes have a distinct spectral signature, especially at short visible wavelengths, compared to naturally turbid waters. These findings should help develop a robust algorithm to identify and map dredge plumes in coastal waters using satellite imagery.

Author Contributions: Conceptualization, E. K.; methodology, E.K., L.DK, R.M. and N.V.; laboratory analyses, I.M., A.S. and D.D.; satellite imagery analysis, L.DK, D.D. and E.K.; writing—original draft preparation, D.D., L. DK. and E.K.; writing—review and editing, D.D., L. D.K. and E.K.; project administration, and funding acquisition, E.K. All authors have read and agreed to the published version of the manuscript.

Funding: This research was funded by ESA, ESA Contract No. 4000143932/24/I-DT-bgh.

Data Availability Statement: Part of the data can be made available on request.

Acknowledgments: This research was performed in the framework of the PLUMES (ESA) project, Contract No. 4000143932/24/I-DT-bgh. The authors would like to thank DEME for their support during the project, so as G. Neukermans et al. (Univ. Gent) for their help in terms of laboratory analyses.

Conflicts of Interest: The authors declare no conflicts of interest.

Abbreviations

The following abbreviations are used in this manuscript:

AOT	Aerosol Optical Thickness
Chla	Chlorophyll-a
CSD	Cutter Suction Dredgers
ECMWF	European Centre for Medium-Range Weather Forecasts
EO	Earth Observation
FNU	Formazin Nephelometric Unit
HPLC	high-performance liquid chromatography
IOCCG	International Ocean Colour Coordinating Group

 doi:10.20944/preprints202602.0865.v1

LOV	Laboratoire d'Océanographie de Villefranche
LUT	look-up tables
MSI	Multi-Spectral Imager
NRT	Near Real Time
NIR	near-infrared
OLI	Operational Land Imager
S2	Sentinel-2
SIMEC	SIMilarity Environment Correction
SPM	Suspended Particulate Matter
TSHD	Trailing Suction Hopper Dredgers
TOA	Top-of-Atmosphere
VNIR	visible and near-infrared

Appendix A

Supplementary Figures

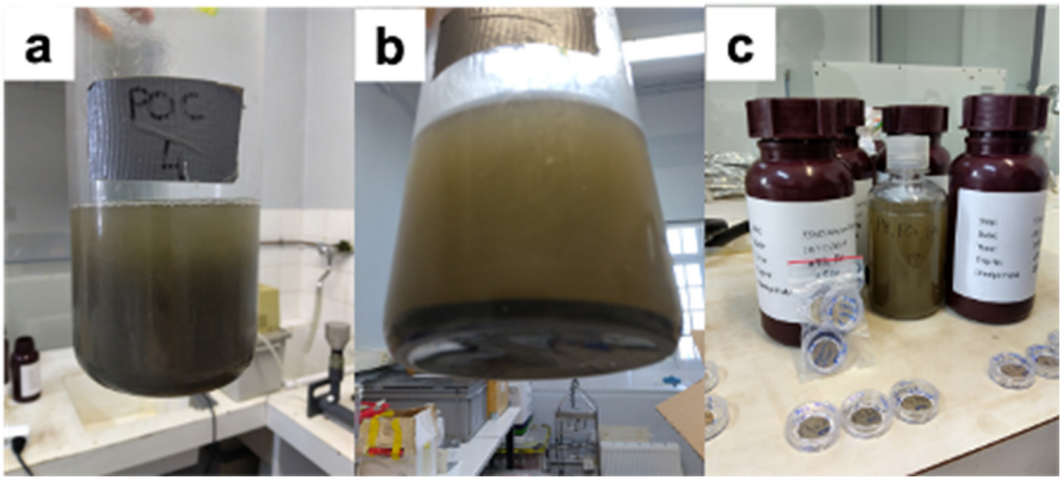

Figure A1. Typical water samples collected in the first European dredge site (D1EU). Water samples were first transferred to transparent bottles and mixed (a) to avoid deposits (b) before filtrations to determine SPM concentration (in triplicates), particulate organic and inorganic fractions (in triplicates), identify and quantify phytoplankton pigments and measure particulate light absorption (c).

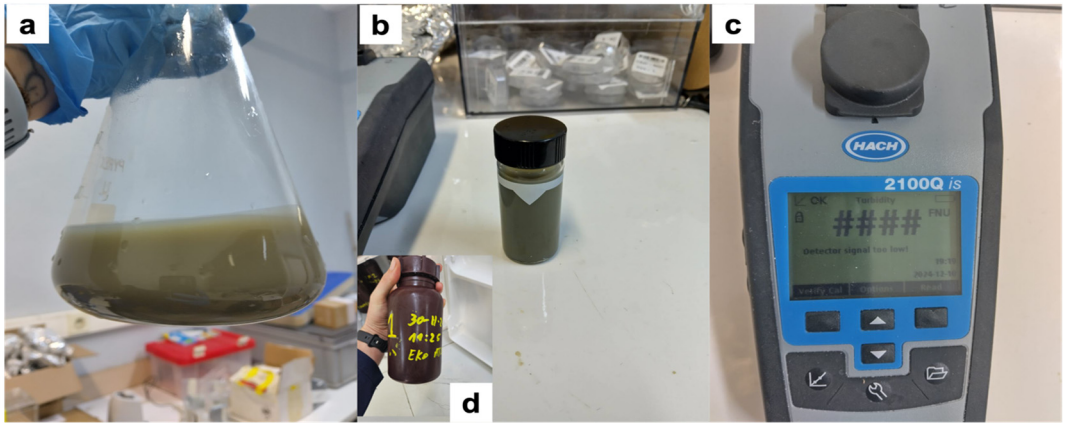

 doi:10.20944/preprints202602.0865.v1

Figure A2. Typical water samples collected in the African dredge site (DA1). Water samples were first transferred to transparent bottles and mixed (a), transferred to vials (b) to measure water turbidity (c). Beyond the upper limit of 1000 FNU, the original water sample (d) was diluted in Milli-Q water prior to laboratory analyses.

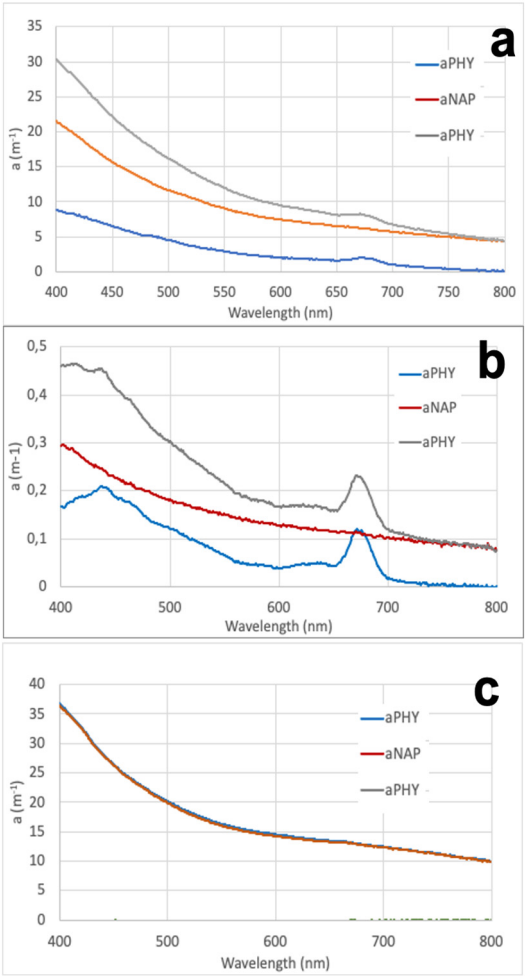

Figure A3. Typical light absorption coefficients of total (ap), algal (aPHY) and non-algal (aNAP) particles in suspension in water samples collected in the dredge plumes: European sites D1EU (a) and D2EU (b), African site D1A (c). These typical spectra notably highlight the potential significant contribution of algal particles.

 doi:10.20944/preprints202602.0865.v1

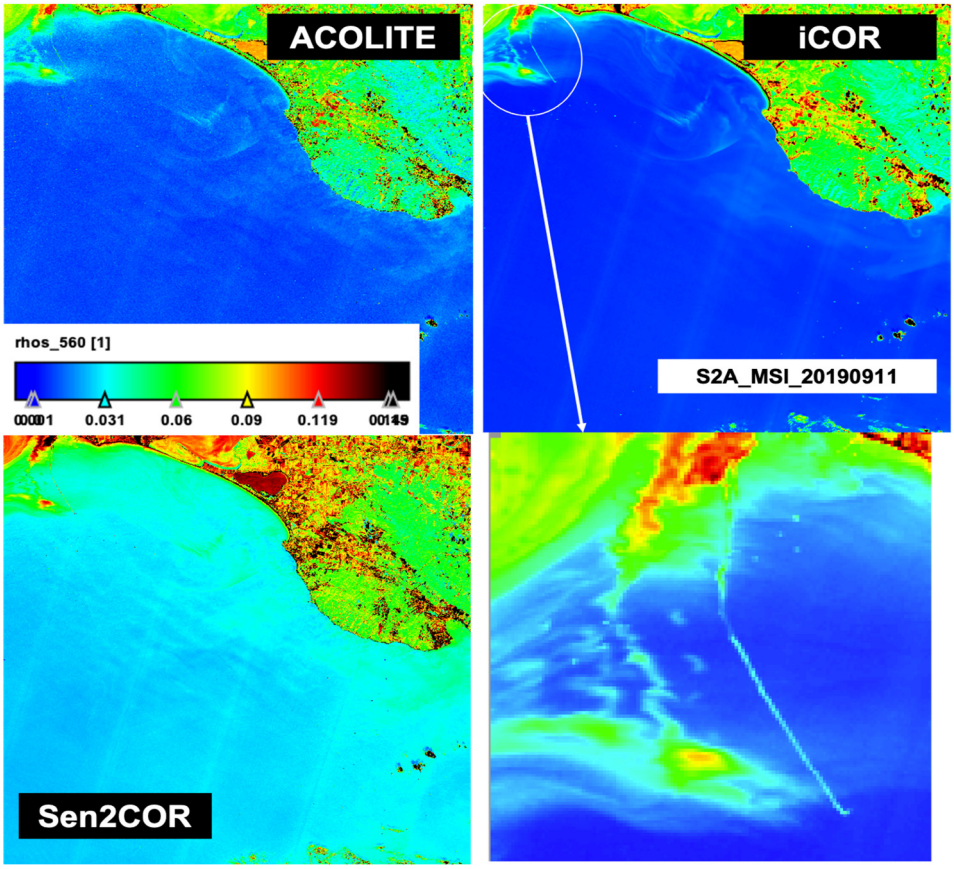

Figure A4. Example of selected S2-MSI image (S2A-20190911) showing dredge plumes processed from L1C using the ACOLITE (left) and iCOR (right) processors. The product shown with the same colour scale is the aquatic reflectance at 560 nm. The test site is in Russia.

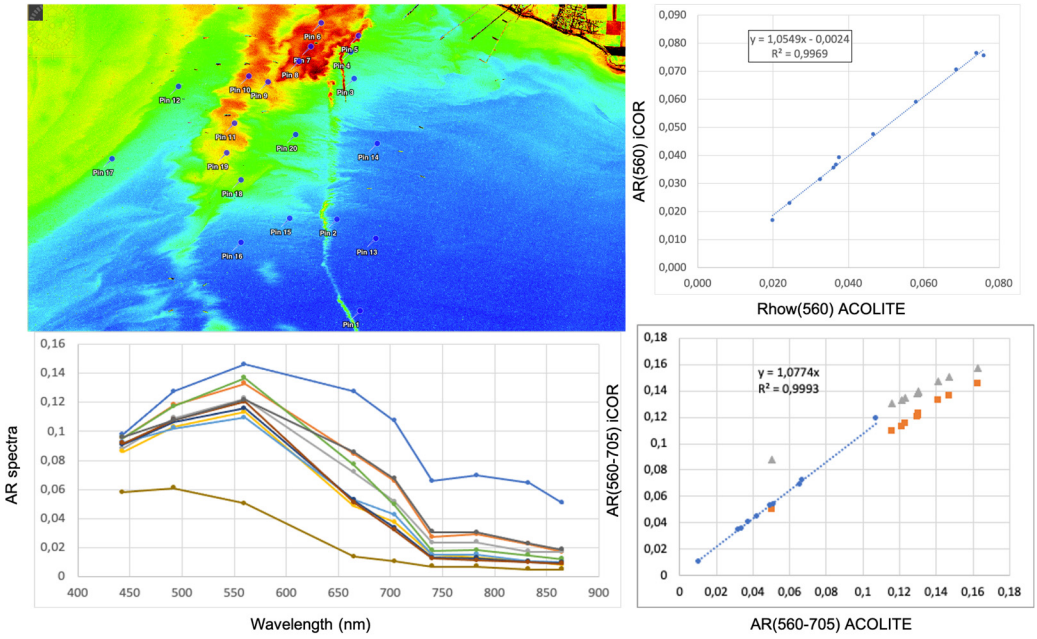

Figure A5. Typical intercomparisons (spectra and scatterplots) between S2-MSI AR values in and outside dredge plumes obtained from iCOR and ACOLITE processors. Considered test sites are located in Mexico, Russia, Africa and UK.

 doi:10.20944/preprints202602.0865.v1

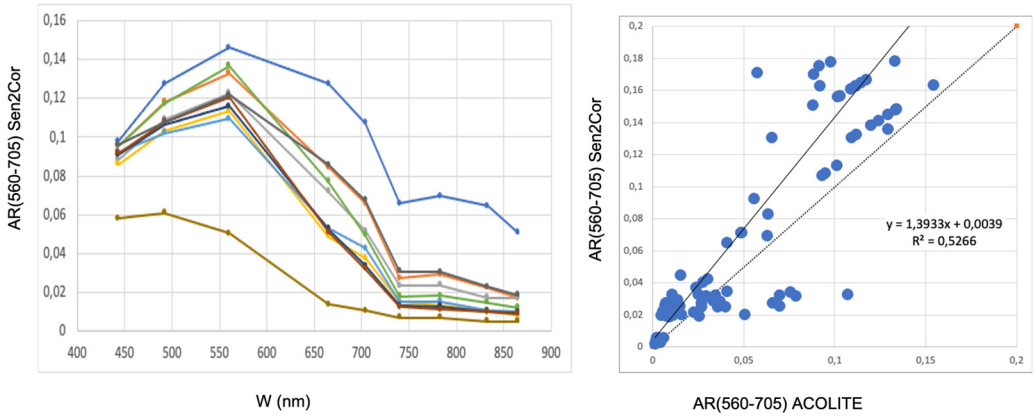

Figure A6. Typical intercomparisons (spectra and scatterplots) between S2-MSI AR values in and outside dredge plumes obtained from Sen2Cor and ACOLITE processors. Considered test sites are located in Mexico, Russia, Africa and the UK.

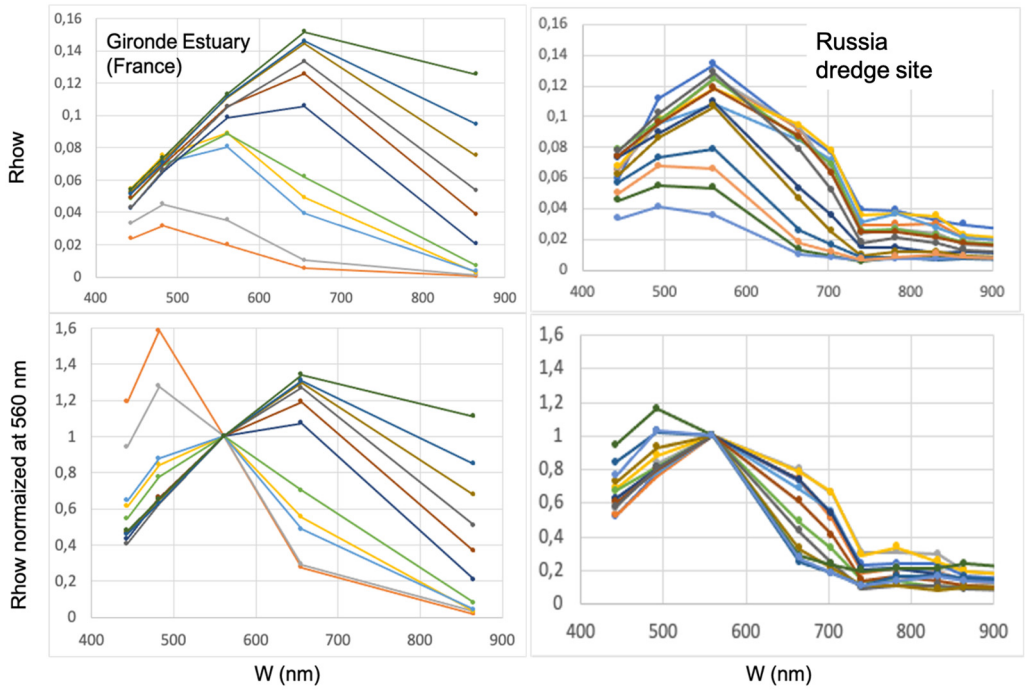

Figure A7. Typical ACOLITE-derived AR spectra respectively extracted from L8-OLI and S2-MSI satellite data in (highly) turbid waters of the Gironde Estuary (left) and Russia dredge site (right). The bottom panels show the same spectra normalized at 560 nm).

 doi:10.20944/preprints202602.0865.v1

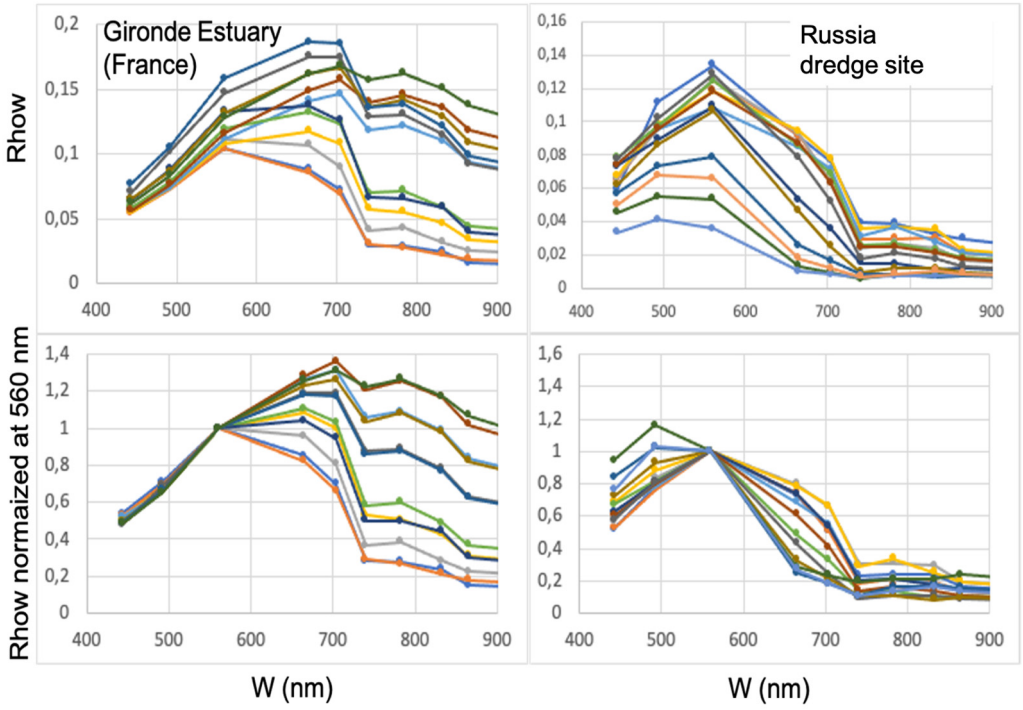

Figure A8. Typical ACOLITE-derived AR spectra respectively extracted from L8-OLI and S2-MSI satellite data in (highly) turbid waters of the Gironde Estuary (left) and Russia dredge site (right). The bottom panels show the same spectra normalized at 560 nm).

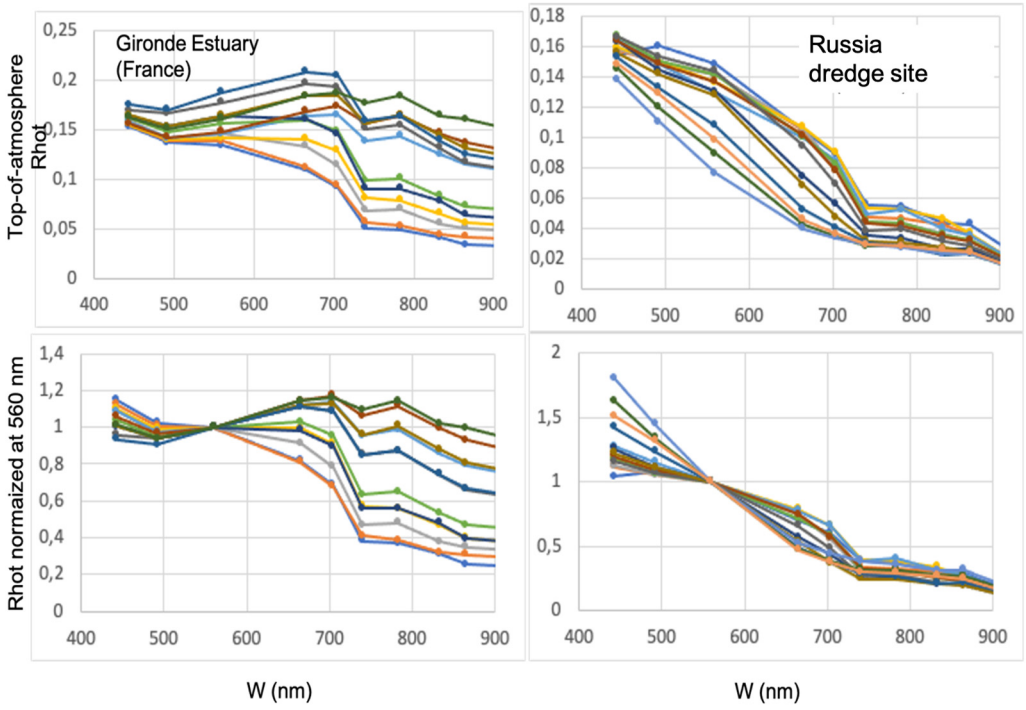

Figure A9. Typical ACOLITE-derived top-of-atmosphere Rhot spectra extracted from S2-MSI satellite data in (highly) turbid waters of the Gironde Estuary (left) and Russia dredge site (right). The bottom panels show the same spectra normalized at 560 nm.

 doi:10.20944/preprints202602.0865.v1

Appendix B

Supplementary Table

Table A1. Typical Biogeochemical and optical properties of suspended particles in the European (D1EU and D2EU) and African (D1A) dredge sites, including water samples collected in the hopper, based on laboratory analyses of collected water samples. Statistical values for each site are reported based on minimum, maximum and mean values over the analyzed datasets. See the text for more details.

Parameter **min/max/mean**	PIF (%)	TU/SPM (FNU.m^3.g^{-1})	$a_{nap}/a_p(443)$ (%)	$a_{nap}(443)$/SPM (m^2.g^{-1})	S_{nap} (nm^{-1})
D1EU	89/95/93	0,7/1,1/0,9	89/95/93	0,021/0,067/0,035	0,007/0,009/0,008
D2EU	77/83/89	0,3/0,5/0,7	53/67/88	0,016/0,026/0,037	0,007/0,008/0,007
D1A	86/89/87	0,7/1,1/0,9	86/100/98	0,034/0,041/0,036	0,008/0,010/0,009

References

1. Barnes, B.B.; Hu C., Kovach, C.X., Silverstein, R.N. Sediment plumes induced by the Port of Miami dredging: Analysis and interpretation using Landsat and MODIS data. *Remote Sens. Env.* **2015**, *170*, 328-339, https://doi.org/10.1016/j.rse.2015.09.023.
2. Caballero, I.; Navarro, G.; Ruiz, J. Multi-platform assessment of turbidity plumes during dredging operations in a major estuarine system. *Int. J. Appl. Earth Obs. Geoinf* **2018**, *68*, 31-41, https://doi.org/10.1016/j.jag.2018.01.014.
3. Vlasblom, W.J. Introduction to Dredging Equipment. In *Dredging Equipment and Technology*, University lecture notes, 2003 https://www.dredging.org/dredging-equipment-and-technology/53.
4. Dogliotti, A.I.; Ruddick, K.G.; Nechad, B.; Doxaran, D.; Knaeps, E. A single algorithm to retrieve turbidity from remotely sensed data in all coastal and estuarine waters. Remote Sens. Env. **2015**, *156*, 157–168.
5. Neukermans, G.; Ruddick, K.G.; Loisel, H; Roose, P. Optimization and quality control of suspended particulate matter concentration measurement using turbidity measurements. *Limnol. Oceanogr. Methods* **2012**, *10(12)*, https://doi.org/10.4319/lom.2012.10.1011.
6. Doxaran, D.; Ehn, J.; Bélanger, S.; Matsuoka, A.; Hooker, S.; Babin, M. Optical characterisation of suspended particles in the Mackenzie River plume (Canadian Arctic Ocean) and implications for ocean colour remote sensing. *Biogeosciences* **2012**, 9, 3213-3229, doi:10.5194/bg-9-3213-2012.
7. Rontani, J.F.; Charriere, B.; Sempéré, R.; Doxaran, D.; Vaultier, F.; Vonk, J.E.; Volkman, J.K. Degradation of sterols and terrestrial organic matter in waters of the Mackenzie Shelf, Canadian Arctic. *Organic Geochemistry* **2014**, *75*, 61–73.
8. Chaves, J.E.; Cetinić, I.; Dall'Olmo, G.; Estapa, M.; Gardner, W.; Goñi, M.; Graff, J.R.; Hernes, P.; Lam, P.J.; Liu, Z.; Lomas, M.W.; Mannino, M.; Novak, M.G.; Turnewitsch, R.; Werdell, P.J.; Westberry, T.K. Particulate Organic Matter Sampling and Measurement Protocols: Consensus Towards Future Ocean Color Missions, **2021**, IOCCG Ocean Optics and Biogeochemistry Protocols for Satellite Ocean Colour Sensor Validation, Volume 6.0, IOCCG, Dartmouth, NS, Canada.
9. Ras, J.; Claustre, H.; Uitz, J. Spatial variability of phytoplankton pigment distributions in the Subtropical South Pacific Ocean: comparison between in situ and modelled data. *Biogeosciences* **2008**, *5*, 353-369, doi: 10.5194/bg-5-353-2008.
10. Boss, E.; D'Sa, E.J.;, Freeman, S.; Fry, E.; Mueller, J.L.; Pegau, S.; Reynolds, R.A.; Roesler, C.; Rottgers, R.; Stramski, D.; Twardowski, M.; Zaneveld, J.R.V. Inherent Optical Property Measurements and Protocols: Absorption Coefficient, Neeley, A. R. and Mannino, A. (eds.), IOCCG Ocean Optics and Biogeochemistry Protocols for Satellite Ocean Colour Sensor Validation, **2018**, Volume 1.0, IOCCG, Dartmouth, NS, Canada.
11. Estapa, M.L.; Boss, E.; Mayer, L.M.; Roesler, C. Role of iron and organic carbon in mass-specific light absorption by particulate matter from Louisiana coastal waters. *Limnol. Oceanogr*. **2012**, *57*, 97–112, doi:10.4319/lo.2012.57.1.0097.

12. Babin, M.; Stramski, D.; Ferrari, G.M.; Claustre, H.; Bricaud, A.; Obolensky, G.; Hoepffner, N. Variations in the Light Absorption Coefficients of Phytoplankton, Non-algal particles, and dissolved organic matter in coastal waters around Europe, *J. Geophys. Res.*, **2003**, *108*, 3211, https://doi.org/10.1029/2001JC000882.
13. Mostafa, Y.E.S. Environmental impacts of dredging and land reclamation at Abu Qir Bay, Egypt. *Ain Shams Eng. J.*, **2012**, *3(1)*, 1-15. https://doi.org/10.1016/j.asej.2011.12.004.
14. Emam, W.M.; Saad, A.E.-H.A.; El-Moselhy, K.M.: Owen, N.A. Evaluation of water quality of Abu-Qir Bay, Mediterranean coast, Egypt. *Int. J. Env. Sci. and Eng.*, **2013**, *4*, 47-54.
15. Lednicka, B.; Kubacka, M.; Freda, W.; Haule, K.; Dembska, G.; Galer-Tatarowicz, K.; Pazikowska-Sapota, G. Water Turbidity and Suspended Particulate Matter Concentration at Dredged Material Dumping Sites in the Southern Baltic. *Sensors*, **2022**, *22(20)*, 8049. https://doi.org/10.3390/s22208049.
16. De Keukelaere, L.; Sterckx, S.; Adriaensen, S.; Knaeps, E.; Reusen, I.; Giardino, C.; Bresciani, M.; Hunter, P.; Neil, C.; Van der Zande, D.; Vaiciute, D. Atmospheric correction of Landsat-8/OLI and Sentinel-2/MSI data using iCOR algorithm: validation for coastal and inland waters, *Eur. J. Remote Sens.*, **2018**, *51*, 525-542, DOI: 10.1080/22797254.2018.1457937.
17. Vanhellemont, Q. Adaptation of the dark spectrum fitting atmospheric correction for aquatic applications of the Landsat and Sentinel-2 archives. *Remote Sens. Env.*, **2019**, *225*, 175–192, https://doi.org/10.1016/j.rse.2019.03.010.
18. Main-Knorn, M.; Pflug, B.; Louis, J.; Debaecker, V.; Müller-Wilm, U.; Ferran, G. Sen2Cor for Sentinel-2. *Image and Signal Processing for Remote Sensing Conference*, **2017**, 3. 10.1117/12.2278218.
19. Doxaran, D.; ElKilani, B.; Corizzi, A.; Goyens, C. Validation of satellite-derived water-leaving reflectance in contrasted French coastal waters based on HYPERNETS field measurements. Frontiers Remote Sens., **2024**, *4*, 1290110.
20. Guanter, L.; Gómez-Chova, L.; Moreno, J. Coupled retrieval of aerosol optical thickness, columnar water vapor and surface reflectance maps from ENVISAT/MERIS data over land. *Remote Sens. Env.*, **2008**, *112(6)*, 2898-2913.
21. Morcrette, J.-J.; Boucher, O.; Jones, L.; Salmond, D.; Bechtold, P.; et al. Aerosol analysis and forecast in the European Centre for Medium-Range Weather Forecasts Integrated Forecast System: Forward modeling. J. Geophys. Res., **2009**, *114* (D6), https://doi.org/10.1029/2008JD011235.
22. Inness, A.; Ades, M.; Agustí-Panareda, A.; Barré, J.; Benedictow, A.; Blechschmidt, A.M.; Suttie, M. The CAMS reanalysis of atmospheric composition. *Atmos. Chem. Phys.*, **2019**, *19(6)*, 3515-3556.
23. Sterckx, S.; Knaeps, S.; Kratzer, S.; Ruddick, K. SIMilarity Environment Correction (SIMEC) applied to MERIS data over inland and coastal waters. *Remote Sens. Env.*, **2015**, *157*, 96-110.
24. Luo, Y.; Doxaran, D.; Ruddick, K.G.; Shen, F.; Gentili, B.; Yan, L.; Huang, H. Saturation of water reflectance in extremely turbid media based on field measurements, satellite data and bio-optical modelling. *Opt. Express*, **2018**, *26(8)*, doi.org/10.1364/OE.26.010435.
25. Doxaran, D.; Ehn, J.; Bélanger, S.; Matsuoka, A.; Hooker, S.; Babin, M. Optical characterisation of suspended particles in the Mackenzie River plume (Canadian Arctic Ocean) and implications for ocean colour remote sensing. *Biogeosciences*, **2012**, *9*, 3213-3229, doi:10.5194/bg-9-3213-2012.
26. Knaeps, E.; Ruddick, K.G.; Doxaran, D.; Dogliotti, A.I.; Nechad, B.; Raymaekers, D.; Sterckx, S. A SWIR based algorithm to retrieve Total Suspended Matter in highly turbid waters. *Remote Sens. Env.*, **2015**, *168*, 66–79.
27. Jafar-Sidik, M.; Gohin, F.; Bowers, D.; Howarth, J.; Hull, T. The relationship between Suspended Particulate Matter and Turbidity at a mooring station in a coastal environment: consequences for satellite-derived products. *Oceanologia*, **2017**, *59(3)*, 365-378.
28. Knaeps, E.; Doxaran, D.; Dogliotti, A.I.; Nechad, B.; Ruddick, K.G.; Raymaekers, D.; Sterckx, S. The SeaSWIR dataset. *Earth Syst. Sci. Data*, **2018**, 10, 1439–1449.

 doi:10.20944/preprints202602.0865.v1

author(s) and contributor(s) and not of MDPI and/or the editor(s). MDPI and/or the editor(s) disclaim responsibility for any injury to people or property resulting from any ideas, methods, instructions or products referred to in the content.